© 2014. Published by The Company of Biologists Ltd | Development (2014) 141, 17-27 doi:10.1242/dev.089078

RESEARCH ARTICLE

STEM CELLS AND REGENERATION

FOXD1 promotes nephron progenitor differentiation by repressing decorin in the embryonic kidney

Jennifer L. Fetting[1], Justin A. Guay[1], Michele J. Karolak[1], Renato V. Iozzo[2], Derek C. Adams[1], David E. Maridas[1], Aaron C. Brown[1] and Leif Oxburgh[1,*]

ABSTRACT

Forkhead transcription factors are essential for diverse processes in early embryonic development and organogenesis. *Foxd1* is required during kidney development and its inactivation results in failure of nephron progenitor cell differentiation. *Foxd1* is expressed in interstitial cells adjacent to nephron progenitor cells, suggesting an essential role for the progenitor cell niche in nephrogenesis. To better understand how cortical interstitial cells in general, and FOXD1 in particular, influence the progenitor cell niche, we examined the differentiation states of two progenitor cell subtypes in *Foxd1*$^{-/-}$ tissue. We found that although nephron progenitor cells are retained in a primitive CITED1-expressing compartment, cortical interstitial cells prematurely differentiate. To identify pathways regulated by FOXD1, we screened for target genes by comparison of *Foxd1* null and wild-type tissues. We found that the gene encoding the small leucine-rich proteoglycan decorin (DCN) is repressed by FOXD1 in cortical interstitial cells, and we show that compound genetic inactivation of *Dcn* partially rescues the failure of progenitor cell differentiation in the *Foxd1* null. We demonstrate that DCN antagonizes BMP/SMAD signaling, which is required for the transition of CITED1-expressing nephron progenitor cells to a state that is primed for WNT-induced epithelial differentiation. On the basis of these studies, we propose a mechanism for progenitor cell retention in the *Foxd1* null in which misexpressed DCN produced by prematurely differentiated interstitial cells accumulates in the extracellular matrix, inhibiting BMP7-mediated transition of nephron progenitor cells to a compartment in which they can respond to epithelial induction signals.

KEY WORDS: Kidney development, Interstitial cell, Progenitor niche, Organogenesis, Mouse

INTRODUCTION

Forkhead transcription factors regulate fundamental biological functions, including fertility, metabolism and immunity (Behr et al., 2007; Fontenot et al., 2003; Nakae et al., 2002; Shih et al., 1999). During embryogenesis, they are required for node and notochord formation and organogenesis of multiple systems such as liver, lung, kidney and central nervous system (Ang and Rossant, 1994; Hatini et al., 1996; Lai et al., 2001; Lee et al., 2005; Shu et al., 2005; Wan et al., 2005). This profoundly important and evolutionarily conserved family of transcription factors is defined by similarity of the DNA-binding forkhead domain (Hannenhalli and Kaestner, 2009). DNA-binding motifs are similar for many forkhead transcription factors and functional diversity is determined by flanking domains that interact with distinct co-factors (Gajiwala and Burley, 2000; Overdier et al., 1994; Pierrou et al., 1994). *In vivo* transcriptional targets and mechanisms of regulation have not yet been determined for the majority of forkhead transcription factors, although many family members are known to associate with the Groucho co-repressor (Yaklichkin et al., 2007a; Yaklichkin et al., 2007b). In this article, we focus on understanding the mechanism of action of FOXD1, which is required for kidney development (Hatini et al., 1996; Levinson et al., 2005).

In the developing mouse kidney, *Foxd1* expression is restricted to cortical interstitial cells, which give rise to glomerular mesangial cells and the interstitium of the mature kidney (Hatini et al., 1996; Humphreys et al., 2010). Importantly, this lineage contributes to scarring in experimental chronic kidney injury, and gene expression analysis indicates that *Foxd1* may be dynamically regulated in kidney injury and repair (Humphreys et al., 2010). In the developing mouse metanephros, ablation of cortical interstitium and inactivation of *Foxd1* both result in accumulation of undifferentiated nephron progenitor cells (cap mesenchyme), demonstrating an essential role of the interstitial cell niche in regulating progenitor cell differentiation (Das et al., 2013; Hatini et al., 1996; Levinson et al., 2005).

Cap mesenchyme cells are arranged in a series of compartments (Mugford et al., 2009). Transition from the CITED1+ SIX2+ compartment to the CITED1– SIX2+ compartment sensitizes them to the inductive effects of canonical WNT signaling (Brown et al., 2013). This transition between progenitor compartments depends on SMAD-mediated bone morphogenetic protein (BMP) signaling. We find that the majority of cap mesenchyme cells in *Foxd1*$^{-/-}$ kidneys remain in the CITED1+ compartment, indicating that the initiating step in nephron progenitor differentiation is inhibited. We performed comparative transcriptome analyses of *Foxd1*$^{-/-}$ versus wild-type kidney tissue to identify direct FOXD1 transcriptional targets that may underlie this interesting compartmental skewing, identifying five candidates for which regulation by FOXD1 could be validated in cell culture. The small leucine-rich proteoglycan decorin (DCN) was of particular interest because of its role in modulating growth factor signaling (Iozzo and Schaefer, 2010). To test its role in the *Foxd1*$^{-/-}$ phenotype, we generated *Foxd1;Dcn* compound mutant mice. *Dcn* inactivation partially reversed the blockage in differentiation of CITED1+ progenitors. SMAD-mediated BMP signaling increases in *Foxd1*$^{-/-}$*;Dcn*$^{-/-}$ kidneys, suggesting that elevated DCN reduces SMAD-dependent transition of cap mesenchyme cells out of the CITED1+ state in the *Foxd1*$^{-/-}$. Indeed, treatment of primary renal progenitor cells with recombinant DCN blocks BMP-mediated transition of cap mesenchyme cells out

[1]Center for Molecular Medicine, Maine Medical Center Research Institute, 81 Research Drive, Scarborough, ME 04074, USA. [2]Department of Pathology, Anatomy and Cell Biology, the Cancer Cell Biology and Signaling Program, Kimmel Cancer Center, Thomas Jefferson University, Philadelphia, PA 19107, USA.

*Author for correspondence (oxburl@mmc.org)

Received 31 August 2012; Accepted 30 September 2013

Development (2014) doi:10.1242/dev.089078

of the CITED1+ state and inhibits epithelial induction. These findings provide a novel mechanism for the skewing of progenitor compartments in the *Foxd1*$^{-/-}$ whereby loss of FOXD1 leads to de-repression of *Dcn* in cortical interstitial cells, resulting in DCN accumulation in the nephrogenic zone, which blocks the differentiation of CITED1+ cap mesenchyme cells.

RESULTS

Cap mesenchyme cells accumulate in the earliest progenitor cell compartment in *Foxd1*$^{-/-}$ embryonic kidneys

The *Foxd1*$^{-/-}$ kidney lacks epithelial differentiation at embryonic day (E) 12.5-15.5, with dramatic expansion of the PAX2+ cap mesenchyme surrounding mislocalized collecting duct (CD) tips (Hatini et al., 1996; Levinson et al., 2005). Cells within the cap mesenchyme are subdivided into distinct compartments (Brown et al., 2013; Mugford et al., 2009). Functional analyses indicate that the compartment expressing CITED1 and SIX2 is refractory to WNT-mediated epithelial induction by the CD, whereas the more distal compartment that loses CITED1 while maintaining SIX2 is sensitized to WNT-mediated induction (Brown et al., 2013). It is not known in which of these compartments progenitor cells are retained in the *Foxd1*$^{-/-}$, or if they maintain a normal distribution across compartments. Therefore, we compared expression of CITED1 and SIX2 between wild-type and *Foxd1*$^{-/-}$ kidneys at E15.5. CITED1 localizes to cap mesenchyme adjacent to the CD tips at the cortex of wild-type kidneys (Fig. 1A). By contrast, CITED1 is expressed in large mesenchymal cell aggregates surrounding CDs throughout the kidney in mutants (Fig. 1B). SIX2 is expressed throughout the cap mesenchyme and pretubular aggregates of wild-type kidneys. In the mutant, mesenchymal clusters surrounding CD tips are SIX2+ (Fig. 1D). These data show that nephron progenitor cells in the *Foxd1*$^{-/-}$ are maintained in the CITED1+ state (Fig. 1C).

During normal development, cortical interstitial cells of the *Foxd1* lineage lose expression of *Foxd1* and differentiate to medullary interstitium and pericytes, including mesangial cells (Humphreys et al., 2010). However, the *Foxd1* locus remains active in interstitial cells of the *Foxd1*$^{-/-}$ (Levinson et al., 2005). To determine whether cortical interstitial cells are blocked in their differentiation similar to cap mesenchyme, we assessed localization of PDGFRβ, which is expressed in medullary interstitium and pericytes (Lindahl et al., 1998) (Fig. 1E). Intriguingly, interstitial cells in the *Foxd1*$^{-/-}$ are PDGFRβ+ irrespective of their cortical or medullary location (Fig. 1F), indicating that these cells are not blocked in their differentiation, but adopt a medullary interstitial cell/pericyte fate.

Foxd1 transcriptome analysis

To explore which genes FOXD1 regulates in the developing kidney, we conducted a transcriptome analysis comparing *Foxd1*$^{-/-}$ and wild-type kidneys using the Affymetrix Mouse Gene 1.0 ST Array. We analyzed RNA from E14.5 *Foxd1*$^{-/-}$ and wild-type littermate kidneys from three biological replicates each containing pooled RNA from two pairs of whole embryonic kidneys from different litters. Data were normalized using XRAY (Biotique Systems). As an initial quality control, we generated a list of differentially expressed candidates (supplementary material Table S2). Genes exceeding 1.5-fold or −1.5-fold difference with a P value <0.05 were considered for further analysis. qRT-PCR was performed on seven candidates using RNA from independent kidney samples, and fold changes were compared with those detected in the microarray analysis (Fig. 2A). All seven transcripts showed an identical directionality of change and a similar fold change by microarray and qRT-PCR, demonstrating the reproducibility of the microarray data in an independent assay.

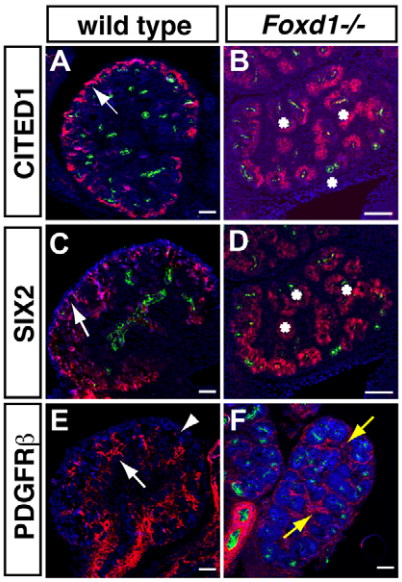

Fig. 1. Marker analysis in the E15.5 *Foxd1*$^{-/-}$ kidney. (A,B) In wild-type kidneys (A), CITED1 (red) localizes to cortical cap mesenchyme cells, whereas *Foxd1*$^{-/-}$ kidneys (B) contain large interior CITED1+ clusters. (C,D) SIX2 (red) localization recapitulates CITED1 staining in both wild-type (C) and *Foxd1*$^{-/-}$ (D) kidneys. (E) Wild-type kidneys contain PDGFRβ+ (red) cells in the medullary interstitium and mesangial cells and exclude PDGFRβ from cortical interstitial cells (arrowhead). (F) *Foxd1*$^{-/-}$ interstitial cells are PDGFRβ+. In all panels, green labels DBA+ CDs and blue labels DAPI+ nuclei. White arrows depict wild-type localization, asterisks depict mislocalized progenitors, and yellow arrows depict aberrant expression in interstitial cells. Scale bars: 100 μm.

Candidate FOXD1 target genes in the cortical interstitium

Foxd1 is expressed in cortical interstitial cells of wild-type kidneys and is downregulated as they differentiate to medullary interstitial cells (Hatini et al., 1996). FOXD1-regulated genes will therefore be differentially expressed in cortical versus medullary interstitial cells, and comparing these two cell types should yield a gene list enriched for FOXD1 targets. We generated a list of 2708 genes by comparing cortical and medullary interstitial cell datasets from GUDMAP (Harding et al., 2011; McMahon et al., 2008) (Fig. 2B). This was subsequently compared with the list of genes differentially regulated between *Foxd1*$^{-/-}$ and wild-type kidneys. Forty-seven overlapping genes were identified and, to further enrich for direct FOXD1 targets, were screened for FOXD1-binding sites within 5 kb upstream of the promoter using Genomatix MatInspector. Five genes containing predicted FOXD1-binding sites were identified: decorin (*Dcn*), zinc finger E-box binding homeobox *2* (*Zeb2*), latent transforming growth factor beta binding protein 1 (*Ltbp1*), discoidin domain receptor family member 2 (*Ddr2*) and collagen type XIV alpha 1 (*Col14a1*). To test the ability of FOXD1 to modulate target gene transcription, we compared gene expression in cells transfected with either the *Foxd1* expression construct CMV-BF2 or with pCX-eGFP. We chose to perform this analysis in MES13 cells because as mesangial cells, they derive from the *Foxd1*-expressing cortical interstitium. Although mesangial cells do not express *Foxd1 in vivo*, qRT-PCR analysis reveals that MES13 cells do express *Foxd1* at a low level, suggesting that they may represent a partially de-differentiated state (supplementary material Fig. S1). We therefore expect genes characteristic of cortical interstitium to be expressed at some level in these cells, and FOXD1 to be able to regulate its

Development (2014) doi:10.1242/dev.089078

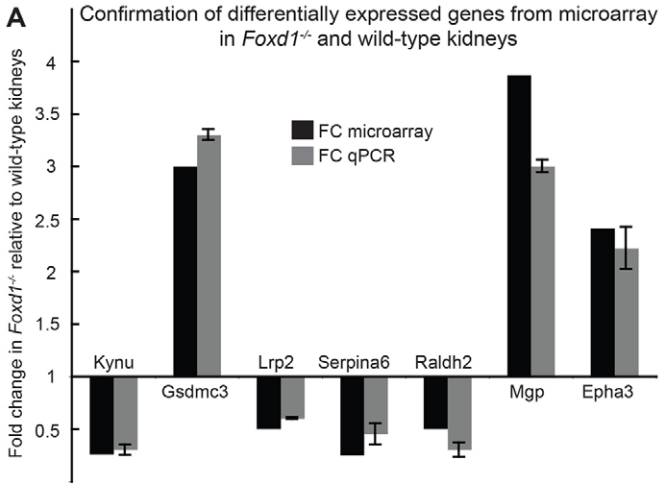

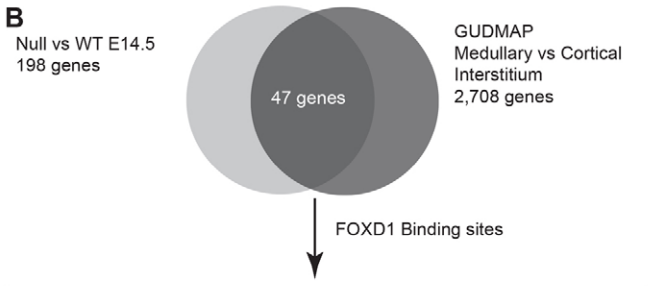

Gene ID	Gene Name	Null vs WT	MI vs CI
Dcn	Decorin	2.49	4.91
Col14a1	Collagen type XIV alpha 1	2.13	3.40
Ltbp1	Latent TGF beta binding protein 1	1.63	4.38
Zeb2	Zinc finger E-box binding homeobox 2	1.49	4.23
Ddr2	Discoidin domain receptor family member 2	1.73	-4.61

* FOXD1 target sites conserved between mouse and human

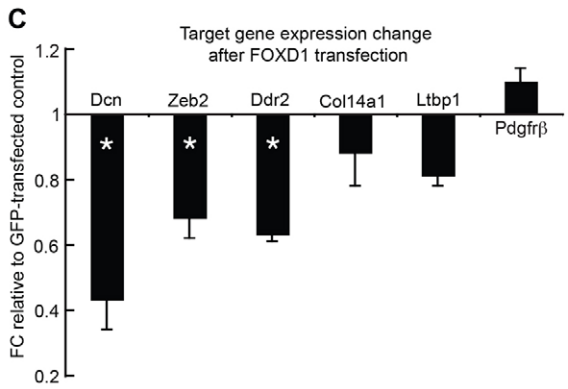

Fig. 2. Screen for candidate FOXD1 targets. (A) Microarray validation. Black bars represent the fold change (FC) in a random selection of differentially expressed genes from the microarray. Gray bars represent average qRT-PCR fold change values in *Foxd1*$^{-/-}$ whole kidney tissue relative to wild-type tissue. qRT-PCR values are normalized to *Gapdh*. (B) Dataset comparisons used to identify target genes. Red text denotes targets with conserved FOXD1-binding sites. CI, cortical interstitium; MI, medullary interstitium; WT, wild type. (C) qRT-PCR of target gene expression in MES13 cells after CMV-BF2 transfection. Bars represent average fold change values in transfected cells, normalized to *Gapdh*, relative to pCX-eGFP transfected cells. Asterisks reflect statistically significant fold changes (P<0.05) as determined by Student's *t*-test. Error bars represent s.d.

targets. We used qRT-PCR to assess the gene expression changes resulting from increased *Foxd1* expression in these cells. Expression of *Dcn*, *Zeb2* and *Ddr2* is significantly reduced upon transfection with *Foxd1* (P<0.05) (Fig. 2C), whereas *Col14a1* and *Ltbp1* levels are essentially unchanged. FOXD1 transfection does not affect expression of the mesangial marker *Pdgfrb*, indicating that gene changes are not due to further de-differentiation.

We focused on *Dcn* because it is both the most highly upregulated of our candidates with a 2.49-fold increase in *Foxd1*$^{-/-}$ kidneys and because its transcription is the most strongly inhibited by FOXD1 in MES13 cells (Fig. 2B,C). Furthermore, comparison of GUDMAP transcriptional profiles of cortical versus medullary interstitial cells shows that *Dcn* expression is elevated 4.9-fold in medullary interstitium, concomitant with loss of *Foxd1* expression (Fig. 2B). To more stringently define *Dcn* regulatory elements, we compared mouse-human orthology of predicted FOXD1-binding sites using the rVista ECR browser. *Dcn* contains two conserved FOXD1-binding sites, and is therefore a strong candidate for direct FOXD1 regulation.

Expression of *Dcn* in the *Foxd1*$^{-/-}$ kidney

To confirm that *Dcn* is misexpressed in interstitial cells *in vivo*, we performed *in situ* hybridization analysis on *Foxd1*$^{-/-}$ and wild-type tissues using a probe against *Dcn*. In the wild-type kidney at E15.5, *Dcn* is expressed at low levels in the cortical interstitium/capsule and at higher levels in the medullary interstitium (Fig. 3A,B). In the E15.5 *Foxd1*$^{-/-}$ kidney, the *Dcn* expression domain is dramatically increased. The entire expanded interstitium surrounding the kidneys expresses high levels of *Dcn*, as does the interstitium surrounding the mislocalized regions of cap mesenchyme (Fig. 3C,D). Neither cap mesenchyme nor the CDs express *Dcn* in either wild-type or *Foxd1*$^{-/-}$ kidneys. Importantly, in the *Foxd1*$^{-/-}$ kidney, *Dcn*-expressing cells surround all of the CITED1+ progenitor cell clusters, whereas in the wild-type kidney these cells are never adjacent to *Dcn* expression.

We then performed immunostaining on whole E14.5 *Foxd1*$^{-/-}$ and wild-type kidneys with an anti-DCN antibody to confirm that the transcriptional misregulation translates into aberrant DCN protein expression. In the wild-type kidney (Fig. 3E), DCN localizes primarily to the medullary interstitium. Little to no DCN can be detected in the cortex, or within glomeruli. By contrast, DCN localizes throughout the *Foxd1*$^{-/-}$ kidney (Fig. 3F). Thus, in the E15.5 *Foxd1*$^{-/-}$ kidney, *Dcn* is misregulated in cortical interstitial cells lacking *Foxd1*. Progenitor differentiation blockage is partially relieved by E17.5 in *Foxd1*$^{-/-}$ kidneys (Levinson et al., 2005). This correlates with a decrease in aberrant *Dcn* expression. Misexpression of *Dcn* is largely confined to the cortex at E17.5, and only a modest number of CITED1+ progenitors abut *Dcn*-expressing cells (supplementary material Fig. S2). DCN associates with collagen I and is predicted to bind collagen IV, modulating their conformation (Fleischmajer et al., 1991; Parkin et al., 2011; Schönherr et al., 1995). We next investigated whether collagens also mislocalize in *Foxd1*$^{-/-}$ kidneys. In wild-type kidneys, both collagens I and IV localize to epithelial basement membranes. Cortical interstitium contains collagen I but not IV (Fig. 3G,H). In *Foxd1*$^{-/-}$ kidneys, collagen I and IV are localized similarly to wild type in epithelial basement membrane, but the interstitium contains both collagens I and IV; thus, unlike wild type, nephron progenitor cells in the mutant reside in a collagen IV-rich environment (Fig. 3I,J).

The data described above led us to investigate if FOXD1 directly represses *Dcn*. Our genome scans identified two species-conserved FOXD1-binding sites, one 4.9 kb upstream of the UCSC genome browser-predicted *Dcn* transcription start site and one 17.5 kb downstream of the 3′UTR. The 5′ FOXD1-binding site

Development (2014) doi:10.1242/dev.089078

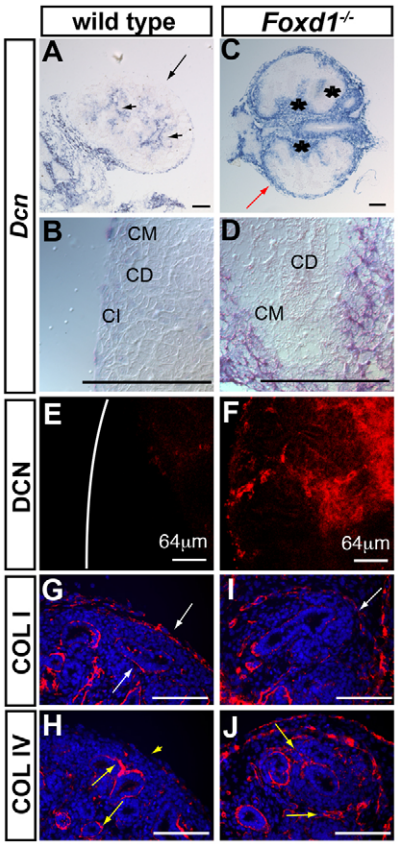

Fig. 3. Extracellular matrix protein mislocalization in E15.5 *Foxd1*$^{-/-}$ kidneys. (A-D) *In situ* hybridization with a probe against *Dcn* in wild-type (A,B) and *Foxd1*$^{-/-}$ (C,D) kidneys. Black arrows and arrowheads depict wild-type cortical and medullary expression, respectively. Red arrows and black asterisks denote aberrant cortical and medullary interstitial expression, respectively. CD, collecting duct; CI, cortical interstitium; CM, cap mesenchyme. (E,F) Optical sections through wild-type (E) and *Foxd1*$^{-/-}$ (F) kidneys. DCN protein (red) localizes to the cortex in *Foxd1*$^{-/-}$ (F). (G,H) In wild-type kidneys, collagen I (red) associates with tubule basement membranes and cortical interstitium (white arrows) (G) and collagen IV (red) associates solely with tubule basement membranes (yellow arrows) and is excluded from cortical interstitium (yellow arrowhead) (H). (I,J) In *Foxd1*$^{-/-}$ kidneys, collagen I localizes to the same compartments as in wild type (white arrow) (I), whereas collagen IV expression is widespread in *Foxd1*$^{-/-}$ interstitium (yellow arrows) (J). Scale bars: 100 μm (A-D,G-J).

is CCAAAGT**CAACA**GG and differs from the TRANSFAC consensus FOXD1-binding site (CTWAWGT**AAACA**NWG) at only three residues, and at none of the five 100% conserved bases (bold) (Pierrou et al. 1994). The 3′ binding site sequence is GATAAA**TAAACA**GT, and it differs from the consensus site at four bases and none of the 100% conserved bases (Fig. 4A,B). To confirm that FOXD1 binds the endogenous sites, we performed a chromatin immunoprecipitation (ChIP) assay using MES13 cells that had been transfected with a triple-FLAG-tagged *Foxd1* expression construct (3xFLAG-FOXD1). 3xFLAG-FOXD1-associated chromatin complexes were compared with complexes from pCX-eGFP transfected cells, and assayed for enrichment of the FOXD1-binding sites in the *Dcn* locus using PCR. There was a sevenfold enrichment of the 5′ binding site in 3xFLAG-FOXD1-transfected cells relative to GFP-transfected control cells and a 2.5-fold enrichment of the 3′ binding site (Fig. 4C). From these data, we conclude that FOXD1 physically associates at the *Dcn* locus.

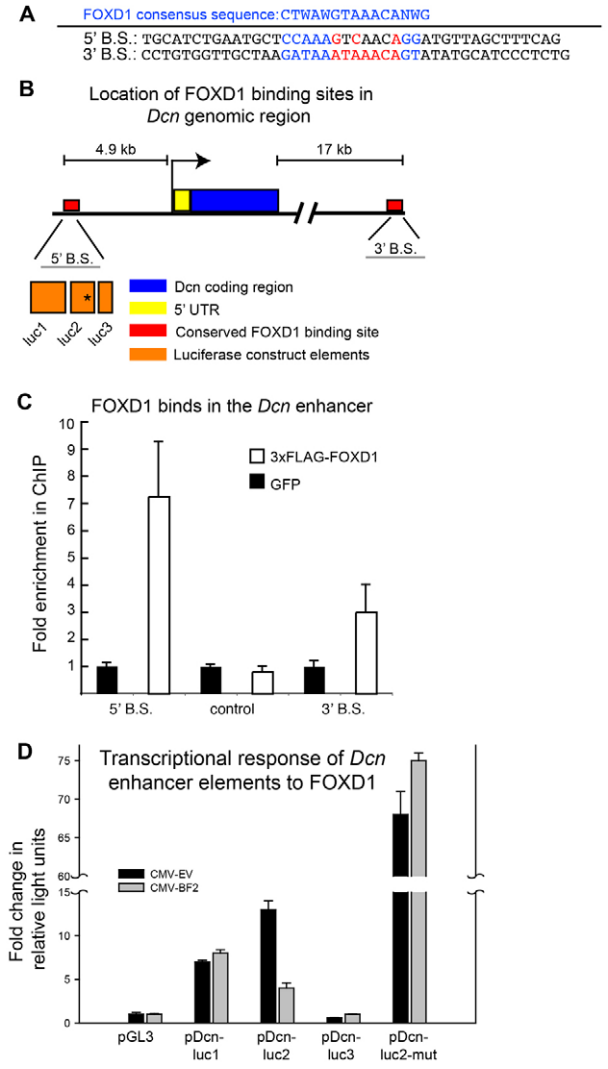

Fig. 4. FOXD1 directly represses *Dcn*. (A) Conserved 5′ and 3′ FOXD1-binding sites with flanking genomic sequence. Blue script denotes consensus FOXD1 sequence. Red script indicates forkhead core sequence. Black script indicates mutated bases in pDcn-luc2-mut. (B) Schematic of species-conserved FOXD1-binding sites adjacent to the *Dcn* locus and enhancer element location. Black asterisk denotes 5′ FOXD1-binding site. (C) Graph of ChIP results. Black bars indicate fold change enrichment from 3xFLAG-FOXD1 samples relative to GFP samples. B.S., binding site. (D) Luciferase assay demonstrating FOXD1-binding site functionality. Bars represent average fold change in relative light units from five replicates compared with PGL3-promoter control. Black and gray bars indicate co-transfection with an empty CMV expression construct and CMV-BF2, respectively. Error bars represent standard error.

Our rVista analysis of the 5′ binding site predicted three orthologously conserved elements, each containing multiple predicted transcription factor-binding sites (supplementary material Table S3). We generated a series of luciferase constructs with each element cloned into a pGL3-promoter vector (Fig. 4D). pDcn-luc2 contains the 5′ FOXD1-binding site. MES13 cells were transfected with pGL3-promoter or one of the three luciferase constructs and co-transfected with either pCDNA3.1 or CMV-BF2. The resulting luciferase activity was measured and compared with pGL3-promoter alone (Fig. 4D). Both pDcn-luc1 and pDcn-luc2 co-transfected with empty CMV vector activate luciferase transcription compared with pGL3 alone, whereas pDcn-luc3 has

Development (2014) doi:10.1242/dev.089078

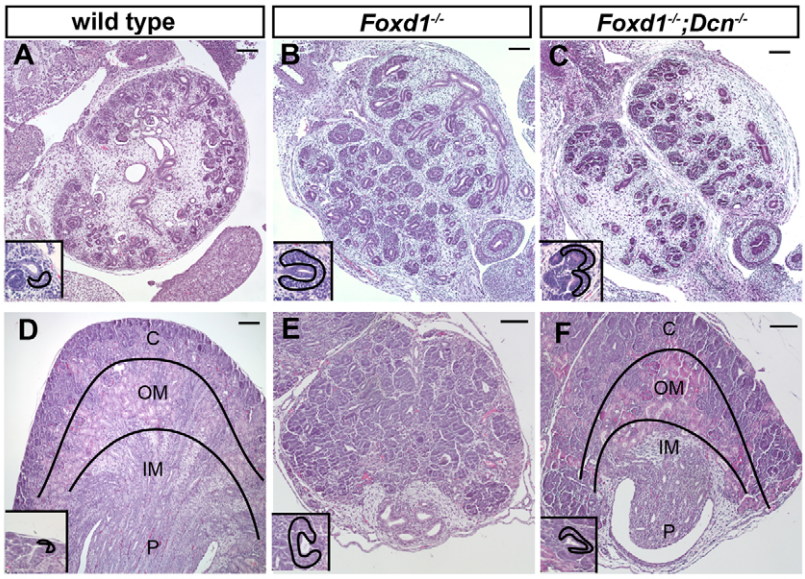

Fig. 5. Genetic ablation of *Dcn* partially rescues the *Foxd1*$^{-/-}$ phenotype. (A-C) Hematoxylin and Eosin (H&E)-stained level-matched sagittal paraffin E15.5 kidneys sections depicting overall kidney organization from wild-type (A), *Foxd1*$^{-/-}$ (B) and *Foxd1*$^{-/-}$;*Dcn*$^{-/-}$ (C) littermates. Insets show nephrogenic units with cap mesenchymes outlined in black. (D-F) Representative sections from five H&E-stained medial transverse paraffin sections from P0 wild-type (D), *Foxd1*$^{-/-}$ (E) and *Foxd1*$^{-/-}$;*Dcn*$^{-/-}$ (F) littermates. Black lines indicate organization into discrete cortical, outer medulla and inner medulla regions. C, cortex; OM, outer medulla; IM, inner medulla; *P*, papilla. Scale bars: 100 µm.

no transcriptional activity. Dcn-luc1 and Dcn-luc2 regions thus appear to contain binding sites for transcriptional activators. Co-transfection of CMV-BF2 did not modulate pDcn-luc1 or pDcn-luc3 expression, but significantly inhibited pDcn-luc2 ($P<2\times10^{-4}$). To confirm that this inhibition requires the FOXD1-binding site, we generated a pDcn-luc2-mut construct in which the forkhead core sequence **TCAACA** was replaced with **CCGGTA** (Fig. 4A). Even in the absence of CMV-BF2, mutating the FOXD1-binding site increased transcriptional activity 68-fold compared with pGL3-promoter alone, suggesting that MES13 expression of FOXD1 or another factor represses pDcn-luc2 transcription through the FOXD1-binding site in MES13 cells. Reporter activity was not decreased by transfection with CMV-BF2, demonstrating that mutagenesis of the FOXD1 site abrogated the repressive activity of FOXD1 (Fig. 4D). Taken together, these data indicate that we have identified a novel enhancer element upstream of *Dcn* where FOXD1 binds and represses transcription.

Partial rescue of the progenitor cell retention phenotype in the *Foxd1*$^{-/-}$ by inactivation of *Dcn*

To reveal if the *Foxd1*$^{-/-}$ phenotype is due to excess DCN, we inactivated *Dcn* on the *Foxd1*$^{-/-}$ background. Litters from *Foxd1*$^{+/-}$;*Dcn*$^{+/-}$ intercrosses were harvested at E15.5 and at postnatal day (P) 0. Cohorts of four E15.5 and five P0 mice for each genotype were compared. Externally, *Foxd1*$^{-/-}$;*Dcn*$^{-/-}$ kidneys resemble the *Foxd1*$^{-/-}$: they are fused and remain attached to the body wall caudal to the location of wild-type kidneys (supplementary material Fig. S3). E15.5 wild-type kidneys demonstrate the expected cortico-medullary organization, with cortically located cap mesenchymes (Fig. 5A). *Foxd1*$^{-/-}$ kidneys are disorganized and have large clusters of cap mesenchymes in the center of the kidney, as previously described (Fig. 5B). However, E15.5 *Foxd1*$^{-/-}$;*Dcn*$^{-/-}$ sections display fewer regions of mislocalized progenitor clusters, and these clusters are smaller (Fig. 5C). This difference is enhanced at P0. Medial transverse sections through pairs of *Foxd1*$^{-/-}$;*Dcn*$^{-/-}$ kidneys indicate that there is partial rescue of *Foxd1*$^{-/-}$ kidney phenotypes. The wild-type P0 kidney is subdivided into functional regions along the kidney's cortico-medullary axis (Fig. 5D): the cortex, the outer medulla, and the inner medulla and papilla. *Foxd1*$^{-/-}$ kidneys lack this arrangement and papillary morphology is rudimentary (Fig. 5E). Characteristic of the *Foxd1*$^{-/-}$ kidney is the inappropriate localization of progenitor cell clusters in all kidney regions. In *Foxd1*$^{-/-}$;*Dcn*$^{-/-}$ kidneys, cortical, outer medullary and inner medullary domains are visible and clear papillary structure and ducts of Bellini can be identified leading to the renal calyx (Fig. 5F). In contrast to the *Foxd1*$^{-/-}$ kidney, progenitor cell clusters are never found in the medulla of the *Foxd1*$^{-/-}$;*Dcn*$^{-/-}$ kidney.

In addition to the recovery of gross patterning, we also saw a change in the size of nephrogenic units in *Foxd1*$^{-/-}$;*Dcn*$^{-/-}$ kidneys compared with *Foxd1*$^{-/-}$. At E15.5, we compared expression of CITED1, which labels nephron progenitor cells, and LEF1, which labels clusters of differentiating pretubular aggregates and renal vesicles, in wild-type, *Foxd1*$^{-/-}$ and *Foxd1*$^{-/-}$;*Dcn*$^{-/-}$ littermate kidneys. In all analyses, CITED1 and LEF1 cell counts were restricted to cells associated with a cross-section through a CD tip with a visible lumen. Wild-type kidneys contain ~16 CITED1+ cells per CD tip in 5-µm sections (Fig. 6A). *Foxd1*$^{-/-}$ kidneys contain ~42 CITED1+ cells per CD tip (Fig. 6B). *Foxd1*$^{-/-}$;*Dcn*$^{-/-}$ CDs associate with significantly fewer, an average of 26 CITED1+ cells ($P<3.3\times10^{-32}$) (Fig. 6C,D). We also quantified the number of LEF1+ cells per cluster in 5-µm sections. In the wild type, LEF1+ clusters contain an average of eight cells (Fig. 6E). *Foxd1*$^{-/-}$ kidneys have clusters with an average of five LEF1+ cells (Fig. 6F). This is rescued in *Foxd1*$^{-/-}$;*Dcn*$^{-/-}$ kidneys, which have clusters with an average of eight LEF1+ cells ($P<5.8\times10^{-17}$) (Fig. 6G,H). Importantly, the ratio of CITED1+ cells:LEF1+ cells, which is 2:1 in wild-type kidneys, increases to 7:1 in *Foxd1*$^{-/-}$ kidneys. These data reflect a decrease in the rate of differentiation from the CITED1+ state to the LEF1+ state in *Foxd1*$^{-/-}$ kidneys compared with wild type. In *Foxd1*$^{-/-}$;*Dcn*$^{-/-}$ kidneys, this ratio is 3:1, indicating that cells progress from the CITED1+ state to the LEF1+ state at nearly the wild-type rate (Fig. 6I).

The same reduction in CITED1+ progenitor cells between littermates is seen at P0. In wild-type kidneys, ~24 CITED1+ cells associate with each CD tip in a 5-µm section (Fig. 6J). However, *Foxd1*$^{-/-}$ CD tips associate with an average of 50 CITED1+ cells (Fig. 6K). The number of CITED1+ cells in *Foxd1*$^{-/-}$;*Dcn*$^{-/-}$ is significantly reduced compared with *Foxd1*$^{-/-}$ (Fig. 6L), with ~30 CITED1+ cells/CD tip ($P<9.8\times10^{-25}$) (Fig. 6M). For each genotype,

Development (2014) doi:10.1242/dev.089078

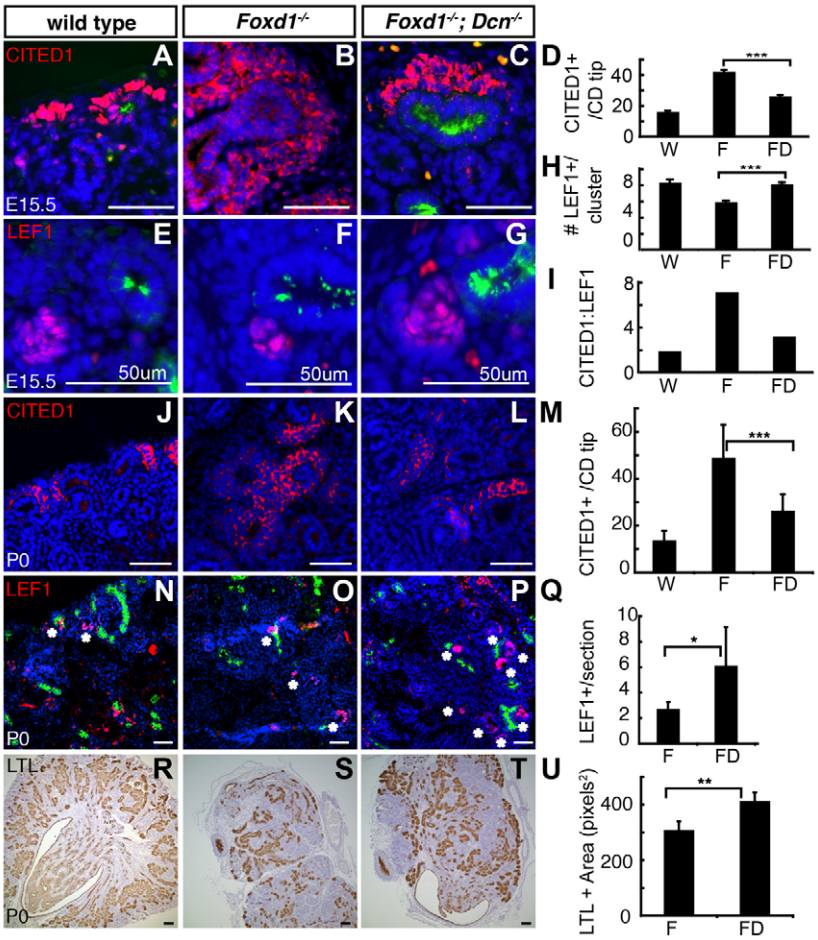

Fig. 6. Genetic ablation of *Dcn* increases nephrogenesis in the *Foxd1*$^{-/-}$ kidney. (A-C) CITED1 (red) staining in E15.5 wild-type (A), *Foxd1*$^{-/-}$ (B) and *Foxd1*$^{-/-}$;*Dcn*$^{-/-}$ (C) nephrogenic units. (D) Quantification of the average number of CITED1+ cells/CD tip with a reduction in the number of CITED1+ cells in *Foxd1*$^{-/-}$;*Dcn*$^{-/-}$ kidneys compared with *Foxd1*$^{-/-}$. $P<2.8\times10^{-47}$ for wild type versus *Foxd1*$^{-/-}$, $P<4.3\times10^{-25}$ for wild type versus *Foxd1*$^{-/-}$;*Dcn*$^{-/-}$, and $P<3.3\times10^{-32}$ for *Foxd1*$^{-/-}$;*Dcn*$^{-/-}$ versus *Foxd1*$^{-/-}$. ***$P<10^{-32}$. *n*=50 CD tips/genotype. (E-G) LEF1 (red) localization in E15.5 wild-type (E), *Foxd1*$^{-/-}$ (F) and *Foxd1*$^{-/-}$;*Dcn*$^{-/-}$ (G) nephrogenic units. (H) Quantification of the average number of LEF1+ cells/cluster. $P<2.2\times10^{-7}$ for wild type versus *Foxd1*$^{-/-}$, $P<0.68$ for wild type versus *Foxd1*$^{-/-}$;*Dcn*$^{-/-}$, and $P<5.8\times10^{-17}$ for *Foxd1*$^{-/-}$ versus *Foxd1*$^{-/-}$;*Dcn*$^{-/-}$. ***$P<10^{-17}$. *n*=50 CD tips/genotype. (I) Graph depicting ratio of CITED1+ cells:LEF1+ cells per CD tip. (J-L) CITED1 (red) localization in P0 wild-type (J), *Foxd1*$^{-/-}$ (K) and *Foxd1*$^{-/-}$;*Dcn*$^{-/-}$ (L) nephrogenic units. (M) Quantification of the average number of CITED1+ cells/CD tip in each genotype. The number of CITED1+ cells decreases by half in the *Foxd1*$^{-/-}$;*Dcn*$^{-/-}$ kidneys. $P<9\times10^{-25}$ for wild type versus *Foxd1*$^{-/-}$, $P<1.7\times10^{-16}$ for wild type versus *Foxd1*$^{-/-}$;*Dcn*$^{-/-}$, and $P<9\times10^{-16}$ for *Foxd1*$^{-/-}$ versus *Foxd1*$^{-/-}$;*Dcn*$^{-/-}$. ***$P<10^{-18}$. *n*=50 CD tips/genotype. (N-P) LEF1 (red) marks renal vesicles (white asterisks) in wild-type (N), *Foxd1*$^{-/-}$ (O) and *Foxd1*$^{-/-}$;*Dcn*$^{-/-}$ (P) kidney sections. Asterisks indicate LEF1+ aggregates. (Q) Graph quantifying the number of LEF1+ structures in *Foxd1*$^{-/-}$ and *Foxd1*$^{-/-}$;*Dcn*$^{-/-}$ kidneys, with a twofold increase seen in the latter. *$P<0.001$. *n*=3 sections from each of five kidneys per genotype. (R-T) Lotus lectin (LTL, brown) labels differentiated proximal tubules in wild-type (R), *Foxd1*$^{-/-}$ (S) and *Foxd1*$^{-/-}$;*Dcn*$^{-/-}$ (T) kidney sections. (U) Graph depicting a 25% increase in the epithelialized area in *Foxd1*$^{-/-}$;*Dcn*$^{-/-}$ kidneys compared with *Foxd1*$^{-/-}$ kidneys. *$P<0.03$. *n*=3 sections from each of five kidneys per genotype. W, wild type; F, *Foxd1*$^{-/-}$; FD, *Foxd1*$^{-/-}$;*Dcn*$^{-/-}$. Throughout, green is DBA and blue is DAPI. Scale bars: 100 µm (A-C,J-T). In all graphs, error bars represent s.d. *P* values were determined using Student's *t*-test. *n*=5 per genotype.

50 CD tips from three non-adjacent sections from each of five kidneys were counted.

This decrease in CITED1+ cells in *Foxd1*$^{-/-}$;*Dcn*$^{-/-}$ kidneys correlates with increased numbers of LEF1+ pretubular aggregates and renal vesicles at P0. In wild-type kidneys, many CD tips in a 5-µm section associate with LEF1+ structures (Fig. 6N). Additional interstitial LEF1 staining surrounds CD trunks in all three genotypes. *Foxd1*$^{-/-}$ kidneys have few LEF1+ pretubular aggregates and renal vesicles per section (Fig. 6O), whereas *Foxd1*$^{-/-}$;*Dcn*$^{-/-}$ kidneys show a sizable increase in the number of LEF1+ structures per kidney section (Fig. 6P). Three sections from each of five kidneys per genotype were quantified, revealing a twofold increase in LEF1+ structures in *Foxd1*$^{-/-}$;*Dcn*$^{-/-}$ compared with *Foxd1*$^{-/-}$ ($P<0.001$) (Fig. 6Q).

An increase in the number of epithelialized nephron structures at P0 would also indicate improved nephron differentiation in the double null. To test this, we assessed localization of the proximal tubule marker lotus lectin. In wild-type kidneys, lotus lectin staining is strongest in proximal tubules in the outer and inner medulla with some weak staining in the CDs in the papilla (Fig. 6R). Lotus lectin staining in *Foxd1*$^{-/-}$ kidneys is strong in scattered regions, but relatively few lotus lectin-positive proximal tubules can be found (Fig. 6S). Increased numbers of lotus lectin-positive structures are seen in *Foxd1*$^{-/-}$;*Dcn*$^{-/-}$ kidneys relative to *Foxd1*$^{-/-}$ (Fig. 6T), with a 25% increase in lotus lectin-positive area ($P<0.03$) (Fig. 6U). Taken together, this marker analysis shows that inactivating *Dcn* in a *Foxd1*$^{-/-}$ background reduces the accumulation of CITED1+ progenitor cells in nephrogenic structures, increases the abundance

Development (2014) doi:10.1242/dev.089078

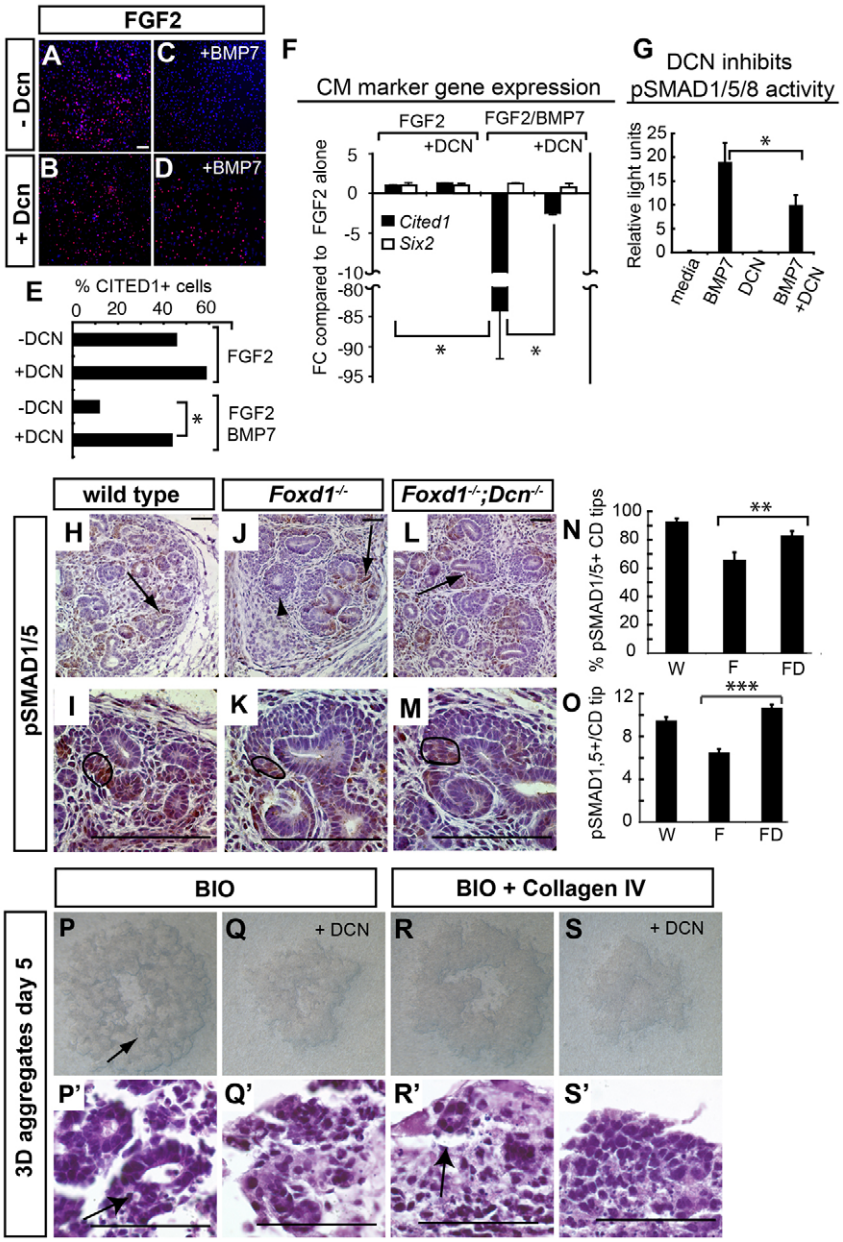

Fig. 7. DCN antagonizes BMP-dependent transition of NZCs out of the CITED1+ compartment. (A-D) CITED1 (red) expression in renal NZC culture in response to treatment with FGF2 (A), FGF2 + DCN (B), FGF2 + BMP7 (C) or FGF2 + DCN + BMP7 (D). (E) Graph quantifying the number of CITED1+ cells in culture. Black bars represent the percentage of CITED1+ cells per DAPI+ nuclei. **P*<0.05. (F) Quantitative RT-PCR of *Cited1* and *Six2* levels in NZCs after growth factor treatment. Bars represent average fold change (FC) values in cells with different treatments relative to FGF2 alone. Changes normalized to *Gapdh*. **P*<0.005. (G) Luciferase assay showing transcriptional response of a BMP7-responsive expression construct. Black bars represent the average relative light units in response to treatment. **P*<0.006. *n*=5 replicates. (H-M) Phospho-SMAD1/5 (brown) labeled wild-type (H,I), *Foxd1*$^{-/-}$ (J,K) and *Foxd1*$^{-/-}$;*Dcn*$^{-/-}$ (L,M) kidney sections. Black arrows indicate pSMAD1/5+ clusters. Black arrowheads indicate pSMAD1/5– clusters. (N) Graph quantifying the percentage of CD tips associated with phospho-SMAD1/5+ depicting a 25% increase in phospho-SMAD1/5+ tips in *Foxd1*$^{-/-}$;*Dcn*$^{-/-}$ sections compared with *Foxd1*$^{-/-}$. ***P*<0.0007. *n*=400 CD tips per genotype. (O) Graph quantifying the average number of phospho-SMAD1/5+ cap mesenchyme cells from level-matched CD tips, indicating a significant increase in the number of phospho-SMAD1/5+ cells in *Foxd1*$^{-/-}$;*Dcn*$^{-/-}$ kidneys compared with *Foxd1*$^{-/-}$ (****P*<9.6×10^{-17}). *n*=150 CD tips per genotype. (P-S) Representative light images of 5-day aggregates of CITED1+ cells treated with BIO alone (P), BIO + DCN (Q), BIO + collagen IV (R) or BIO, collagen IV and DCN (S). (P′-S′) Hematoxylin and Eosin (H&E)-stained sections through the aggregates. Arrows in P-S′ indicate epithelial tubes. *n*=3 for each treatment. W, wild type; F, *Foxd1*$^{-/-}$; FD, *Foxd1*$^{-/-}$;*Dcn*$^{-/-}$. Scale bars: 100 µm. *P* values determined by Student's *t*-test.

of differentiated nephron structures, and improves cortico-medullary patterning of the kidney.

DCN inhibits BMP in cap mesenchyme cells

DCN interacts with TGFβ and receptor tyrosine kinase (RTK) growth factors through diverse mechanisms, including ligand and receptor binding (Neill et al., 2012). Our work indicates that maintaining the CITED1+ progenitor cell state requires RTK signaling and that transition out of the CITED1+ compartment into the SIX2-only compartment requires SMAD-mediated BMP signaling (Brown et al., 2011; Brown et al., 2013). To understand whether DCN retains progenitor cells in the CITED1+ state by modulating either RTK or SMAD signaling pathways, we evaluated the effect of DCN on cultured nephrogenic zone cell (NZC) differentiation (Blank et al., 2009). NZCs were treated with FGF2 to maintain *Cited1* expression, followed by treatment with BMP7 with and without DCN. Changes in *Cited1* expression were measured at both transcript and protein levels. Addition of DCN alone has little effect on the number of CITED1+ cells in FGF2-treated cultures (Fig. 7A,B). However, addition of DCN abrogates the decrease in CITED1+ cells seen upon BMP7 treatment (Fig. 7C,D). Quantification of CITED1+ cells in each condition supports the conclusion that DCN reduces the effect of BMP7 (Fig. 7E), and this is corroborated by gene expression analysis (Fig. 7F). Importantly, although *Cited1* expression is reduced in BMP7-treated cells, the level of *Six2* expression remains the same with or without addition of DCN, indicating that DCN antagonizes BMP7- and SMAD-mediated differentiation of progenitors from the CITED1+ to the SIX2-only compartment.

The pro-differentiative effect of BMP7 relies on Smad1/5/8 transcription factor signaling (Brown et al., 2013). To verify that DCN modulates this pathway, we performed a transcriptional reporter assay in NIH3T3 cells using pBRE-luc, in which luciferase expression is regulated by a Smad1/5/8-binding enhancer element (Korchynskyi and ten Dijke, 2002). DCN antagonizes Smad1/5/8-mediated signaling by BMP7, significantly reducing transcriptional reporter

Development (2014) doi:10.1242/dev.089078

activation (Fig. 7G). These findings suggest that DCN promotes retention of progenitor cells in the undifferentiated CITED1+ compartment by directly antagonizing SMAD-dependent BMP7 signaling. To test the contribution of this interaction to the *Foxd1*$^{-/-}$ phenotype, we compared nuclear phospho-SMAD1/5 expression in wild-type, *Foxd1*$^{-/-}$ and *Foxd1*$^{-/-}$;*Dcn*$^{-/-}$ kidneys at E15.5. In wild-type nephrogenic units, phospho-SMAD1/5 is detected in clusters of cap mesenchyme cells located adjacent to or just under the CD tip (Fig. 7H,I) (Brown et al., 2013). We find that only a subset of CD tips associate with cap mesenchymes containing phospho-SMAD1/5+ cells in the *Foxd1*$^{-/-}$ kidney (Fig. 7J,K), but that this proportion increases in the *Foxd1*$^{-/-}$;*Dcn*$^{-/-}$ kidney (Fig. 7L,M). Quantification of the number of CD tips associated with phospho-SMAD1/5+ cap mesenchymes in five non-adjacent 5-µm sections in each of five pairs of kidneys per genotype revealed that 93% of CD tips associate with phospho-SMAD1/5+ progenitor cells in the wild type compared with 66% in *Foxd1*$^{-/-}$ (P<0.0008) and 83% in *Foxd1*$^{-/-}$;*Dcn*$^{-/-}$ (P<0.0009 versus wild type, P<0.0007 versus *Foxd1*$^{-/-}$; n=400 tips per genotype) (Fig. 7N). To determine if the size of phospho-Smad1/5+ clusters also differs between genotypes, we counted the number of phospho-SMAD1/5+ cap mesenchyme cells per CD tip cross-section (determined by presence of lumens) in these same 5-µm sections. Wild-type kidneys have an average of 9.5 phospho-SMAD1/5+ cap mesenchyme cells per tip, whereas comparable *Foxd1*$^{-/-}$ tips have 6.5 cells (Fig. 7L,M; P<1.6×10^{-9}). By contrast, *Foxd1*$^{-/-}$;*Dcn*$^{-/-}$ kidneys contain 10.7 phospho-SMAD1/5+ cells per CD tip, a significant increase compared with both *Foxd1*$^{-/-}$ and wild-type kidneys (Fig. 7O; P<9.6×10^{-17} and P<0.003, respectively; n=150 CD tips per genotype). These data indicate that DCN reduces SMAD-dependent BMP7 signaling in E15.5 *Foxd1*$^{-/-}$ kidneys.

The hallmark feature of the *Foxd1* null is accumulation of cap mesenchyme cells in the CITED1+ compartment (Fig. 1A,B). To directly test the effect of DCN on differentiation of these cells, we used a three-dimensional culture assay in which tubulogenesis of aggregated CITED1+ cells, which produce endogenous active BMP7, can be induced by the GSK3β antagonist BIO (Brown et al., 2013). CITED1+ cells were aggregated in media with or without recombinant DCN and tubulogenesis was monitored by light microscopy (Fig. 7P-S). BIO-treated aggregates achieve a high level of complexity within 5 days, forming large epithelial structures with lumens (Fig. 7P,P′). However, BIO-treated aggregates cultured with DCN display reduced complexity with few identifiable epithelial structures (Fig. 7Q,Q′), showing that DCN does indeed attenuate differentiation of pure CITED1+ cells in a functional assay, through inhibition of endogenous BMP signaling.

Nephrogenesis is impaired in renal explants grown in dissolved collagen IV (Sebinger et al., 2013). Collagen IV is aberrantly expressed in *Foxd1*$^{-/-}$ kidneys (Fig. 3G,H), such that the extracellular matrix (ECM) environment surrounding the cap mesenchyme cells contains two anti-nephrogenesis factors, collagen IV and DCN. To recapitulate this environment *in vitro*, we cultured BIO-treated aggregates with collagen IV and DCN. Collagen IV alone reduced the complexity of aggregates, and the combination of collagen IV and DCN had the most severe attenuating effect on epithelial differentiation (Fig. 7R-S′). From this, we conclude that we are able to replicate, in culture, part of the aberrant ECM environment found in the *Foxd1*$^{-/-}$ and that this DCN-rich environment prevents the differentiation of epithelial structures.

DISCUSSION

In this study, we identify *in vivo* targets of the FOXD1 transcription factor, and provide a mechanistic explanation for the influence of the interstitial niche on progenitor cell differentiation in the *Foxd1*$^{-/-}$ kidney. FOXD1 represses the gene encoding the small leucine-rich proteoglycan DCN in cortical interstitial cells. When *Foxd1* is inactivated, DCN is expressed and inhibits BMP-SMAD signaling, which blocks transition of the neighboring nephron progenitor cells to a state in which they are susceptible to epithelial induction.

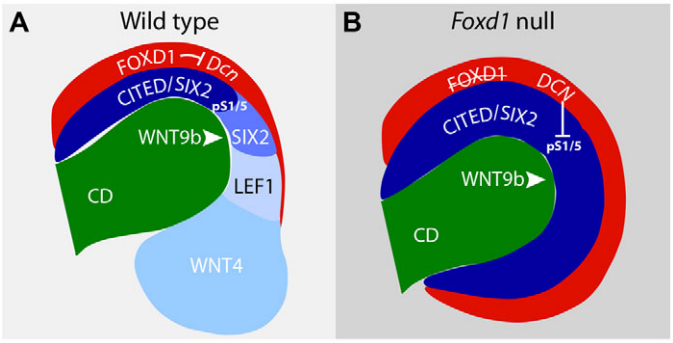

Fig. 8. Model for FOXD1 regulation of nephron progenitor cell differentiation through control of *Dcn* expression. (A) In the wild type, FOXD1 represses *Dcn* in the cortical interstitium. Differentiation of adjacent CITED1+ SIX2+ nephron progenitors to the CITED1– SIX2+ (SIX2+) state that is susceptible to induction by canonical WNT signaling from the collecting duct (CD) requires phospho-SMAD1/5/8 signaling (pS1/5). (B) In the *Foxd1* null, decorin (DCN) is expressed in cortical interstitium, inhibiting phospho-SMAD1/5/8 and preventing transition of CITED1+ SIX2+ cells to the CITED1– SIX2+ state.

The transcriptome analysis for FOXD1 target genes identified surprisingly few signaling molecules. Instead, DAVID pathway analysis of putative FOXD1 target genes revealed that many genes, including *Dcn*, encode ECM proteins that specifically associate with collagen fibril formation, including multiple collagens, fibrillin1 and elastin (Huang et al., 2009a; Huang et al., 2009b). Furthermore, we demonstrated that collagen IV localization is aberrant in *Foxd1*$^{-/-}$ kidneys. This is interesting because it suggests that FOXD1 either directly or indirectly regulates an entire cassette of genes, including *Dcn*, that sets up a specific ECM environment surrounding the cap mesenchyme cells. The importance of ECM components to cellular signaling responses is increasingly evident (Alexi et al., 2011; Schaefer and Iozzo, 2008). In this work, we demonstrate that the aberrant ECM is sufficient to reduce differentiation of progenitor cells to epithelial structures. Stem and progenitor cells, in particular, are sensitive to changes in the ECM environment (Ichii et al., 2012; Mathews et al., 2012a; Mathews et al., 2012b; Wang et al., 2010).

The finding that cap mesenchyme cells are trapped in the CITED1+ compartment in the *Foxd1*$^{-/-}$ kidney is a key observation in this study. Each compartment of the cap mesenchyme differs in its responsiveness to essential signals such as WNTs and BMPs. Progenitor cells respond differently to WNT9b, choosing to proliferate or differentiate depending on whether they have high or low levels of SIX2 (Brown et al., 2013; Karner et al., 2011; Park et al., 2012). In a wild-type kidney, transition out of the CITED1+ state to the SIX2-only state requires BMP7/SMAD signaling (Brown et al., 2013). We propose that DCN reduces BMP/SMAD signaling in *Foxd1*$^{-/-}$ kidneys by modulating both BMP7 and BMP4, expression of which is elevated in this mutant (Levinson et al., 2005). Progenitor cell transition into a WNT9b/β-catenin inducible state is thus prevented (Fig. 8). BMPs are TGFβ superfamily ligands, and their structural similarities suggest that DCN may directly bind BMP7 by the same mechanism as it binds TGFβ1 (Yamaguchi et al., 1990). BMP7 promotes cap mesenchyme cell proliferation through

Development (2014) doi:10.1242/dev.089078

a SMAD-independent mechanism (Blank et al., 2009). Although *Foxd1*$^{-/-}$ kidneys are much smaller than wild-type kidneys, proliferation within cap mesenchyme does not differ significantly, indicating that the effect of BMP on progenitor proliferation is unchanged and suggesting that signaling through SMAD1/5 is specifically affected by DCN (Levinson et al., 2005). Factors governing signaling outcomes of BMP receptor activation are incompletely understood, but include receptor complex conformation at the cell surface, which may be strongly influenced by the extracellular environment (Guzman et al., 2012). Future studies of the molecular mechanism by which DCN acts on BMP ligands and receptors will explore the possibility that it does not simply inhibit BMP signaling, but redirects its outcome.

Our finding that DCN-mediated antagonism of BMP signaling skews progenitor cell compartments in *Foxd1*$^{-/-}$ kidneys suggests that there should be similarities between kidney phenotypes seen upon inactivation of *Bmp7* and *Foxd1*. Although the kidneys of these mutants are morphologically distinct at E14.5, an important similarity is that both mutants retain CITED1-expressing cells and that differentiation to the SIX2-only compartment is blocked (Brown et al., 2013). The *Foxd1* mutant phenotype is highly complex, and our work implicates separate origins of the horseshoe and the progenitor cell retention phenotypes. We speculate that the lack of separation of the *Foxd1*$^{-/-}$ kidney from the body wall imposes severe constraints on the capacity for centrifugal growth of the kidney, compressing CD tips and associated cap mesenchyme cells into a small volume resulting in the characteristic *Foxd1*$^{-/-}$ morphology.

Genetic inactivation of *Dcn* in the *Foxd1*$^{-/-}$ background partially repairs the cortico-medullary patterning defects seen in *Foxd1*$^{-/-}$ kidneys. Intriguingly, BMP signaling is essential for appropriate cortico-medullary patterning, and medullary hypoplasia is seen upon inactivation of the BMP receptor ALK3 (BMPR1A – Mouse Genome Informatics) in the CD (Hartwig et al., 2008; Yu et al., 2009). Thus, in *Foxd1*$^{-/-}$ kidneys, DCN modulation of BMP signaling may inhibit appropriate patterning. An alternative explanation for the *Foxd1*$^{-/-}$ cortico-medullary patterning deficiency is that excess DCN, combined with high levels of the other misexpressed ECM molecules, might form a rigid matrix resulting in a physical impediment to both the outgrowth of the CD tips and the elongation of the CD stalks. Removing DCN from the matrix would reduce its inflexibility, much as loss of *Dcn* reduces the tensile strength of skin, permitting the directional growth of CDs and nephron tubules (Danielson et al., 1997).

The nephrogenic zone has been viewed as a stem cell-stroma niche, in which cortical interstitial support cells promote the self-renewal and/or differentiation of cap mesenchyme cells. However, lineage tracing reveals that cortical interstitial cells are progenitor cells in their own right, which self-renew and differentiate into essential cell types, including mesangial cells and peritubular pericytes (Humphreys et al., 2010). Our gene expression data and PDGFRβ marker analyses reveal that *Foxd1* regulates the progenitor cell status of cortical interstitial cells. Loss of *Foxd1* leads to an increase in transcription of genes normally expressed in cells derived from cortical interstitium, including *Rgs5* and *Mgp* (mesangium) and *Dcn* (medullary interstitium) (supplementary material Table S2). We propose that *Foxd1* acts as a 'stemness' gene for the cortical interstitium, and that in its absence the cortical interstitium prematurely adopts its differentiated fates. The demonstration that interstitium throughout the *Foxd1*$^{-/-}$ kidney expresses PDGFRβ supports this notion. Premature differentiation of cortical interstitial cells correlates with a lack of cap mesenchyme cell differentiation in the *Foxd1*$^{-/-}$ kidney (Fig. 1E,F). We propose that the renal nephrogenic zone comprises a niche composed of interdependent progenitor cell populations, rather than progenitors and stromal support cells. Interestingly, the nephrogenic zone is home to two additional populations of progenitor cells: the *Flk1*+ (*Kdr* – Mouse Genome Informatics) endothelial progenitor cells that give rise to the glomerular capillary tufts, and the *Ret*+ CD tip cells (Chi et al., 2009). Spatial integration of these four stem cell compartments enables the synchronized formation of nephrons containing epithelial cells, endothelial cells and mesangial cells. Defining the axes of communication between these distinct components of the niche is essential for our understanding of nephrogenesis, and for ongoing attempts at *de novo* generation of kidney tissue.

MATERIALS AND METHODS

Mice

Foxd1$^{lacZ/+}$ mice (Hatini et al., 1996) were on an ICR background and *Dcn*^{TM1Ioz} mice (Danielson et al., 1997) on BL/6. Noon of the day of the vaginal plug was designated E0.5. Animal care was in accordance with the National Research Council Guide for the Care and Use of Laboratory Animals and all experiments were approved by the Maine Medical Center IACUC.

Cell culture and treatment

MES13 cells (ATCC Rockville, MD, USA) were maintained per vendor instructions and transfected with CMV-BF2 (kindly provided by E. Lai, Columbia University, NY, USA) using Lipofectamine 2000 (Life Technologies) as per manufacturer instructions. After 24 hours, RNA was prepared using the Qiagen RNeasy Mini Kit. cDNA was synthesized with the qScript cDNA Kit (Quanta BioSciences), and quantitative RT-PCR reactions (three technical replicates) run using iQ Sybr Green SuperMix (Bio-Rad). ICR NZCs were isolated and cultured as described (Blank et al., 2009). Cells were treated with 50 ng/ml FGF2 (R&D Systems) for 6 hours followed by 10 µg/ml DCN (R&D Systems) and/or 50 ng/ml BMP7 (R&D Systems) for 24 hours before immunofluorescence or RNA isolation. NIH3T3 cells (ATCC) were maintained as per vendor instructions. 3D aggregate cultures were isolated and incubated as described (Brown et al., 2013) then treated with 2 µM BIO (Calbiochem), 10 µg/ml DCN and 50 µg/ml collagen IV (BD Biosciences).

Luciferase assays

Conserved elements near the predicted FOXD1-binding site were identified with rVista (rvista.dcode.org). Elements were amplified from genomic DNA using the Phusion High-Fidelity Polymerase Kit (NEB) using primers in supplementary material Table S1.

Amplicons were directionally cloned into pGL3-promoter vector (Promega) using the Fermentas Rapid DNA Ligation Kit. The FOXD1-binding site was mutated using Phusion and the amplicon directionally cloned into pDcn-luc2.

MES13 cells were transfected with either pGL3-promoter or one of the four Dcn-luc constructs along with pRL-CMV (Promega) and either pCDNA3.1 (Life Technologies) or CMV-BF2 as above, incubated for 24 hours with 5% fetal calf serum and luciferase assays were performed using the Dual-Luciferase Reporter Assay Kit (Promega). Five biological replicates were analyzed for each condition.

NIH3T3 cells were transfected with pBRE-luc (Korchynskyi and ten Dijke, 2002) and pRL-CMV (Promega) as above, serum starved for 6 hours, and treated with factors as above. After 24 hours, cells were lysed and luciferase assays were performed as above.

Microarray analysis

Embryonic kidneys were harvested from *Foxd1*$^{-/-}$ and wild-type littermates from three E14.5 litters. Three biological replicates were generated per genotype, each containing two non-littermate kidney pairs. These were pooled and homogenized in Trizol. RNA was prepared using a Qiagen RNeasy Micro Kit. Samples were run on the Affymetrix Mouse Gene 1.0 ST Array platform by the Vermont Genetics Network Microarray

Core Facility. The data discussed in this publication have been deposited in NCBI's Gene Expression Omnibus (Edgar et al., 2002) and are accessible through GEO series accession number GSE52354 (http://www.ncbi.nlm.nih.gov/geo/query/acc.cgi?acc=GSE52354).

Computational analysis

Microarray data were analyzed with XRAY software (Biotique Systems). Genes with at least four probes and $P<0.01$ were selected. FOXD1-binding site analysis was performed using Genomatix MatInspector (genomatix.de) to identify sites with 0.75 matrix similarity to the Transfac V$FREAC4.01 matrix. Binding site conservation was identified via ECR Browser (http://ecrbrowser.dcode.org).

Immunohistochemistry and *in situ* hybridization

Immunostaining was conducted on paraffin sections of paraformaldehyde-fixed tissue as previously described (Blank et al., 2009). Primary antibodies were: CITED1 (1:100; NeoMarkers Cited 1, RB9269-PO; AbCam Cited 1, AB15096); SIX2 (1:50; Santa Cruz Biotechnology SC-67834); PDGFRβ (1:250; Epitomics, 1469-1); collagen IV (1:50; Rockland Antibodies and Assays: 600-401-106-0.1); collagen I (1:50; Rockland Antibodies and Assays: 600-401-103-0.1); DBA lectin (1:250; Vector Laboratories, B-1035); Lotus lectin (1:250; Vector Laboratories, B-1325); phospho-SMAD1/5 (1:50; Cell Signaling Technology, 9516S). Secondary antibodies were: biotinylated anti-rabbit (Vector Laboratories, BA-1000); streptavidin Alexafluor 488 (Life Technologies, S11223); Alexafluor 568 goat anti-rabbit (Life Technologies, A11011); Alexafluor 568 goat anti-mouse (Life Technologies, A11004); Alexafluor 568 donkey anti-goat (Life Technologies, A11057). All secondary antibodies were diluted 1:250. DAPI counterstain was also used (1:10000; Life Technologies D1306).

Methanol-fixed whole E14.5 kidneys were processed as described (Barak and Boyle, 2011) in 1:100 anti-DCN (R&D Systems AF-1060). *In situ* hybridization using digoxigenin-labeled probes was carried out on paraffin sections as described (Oxburgh et al., 2004). PCR amplification from an E17.5 whole-embryo cDNA library was used to generate probe templates.

ChIP

ChIP was performed with pCX-eGFP or p3xFLAG-FOXD1-transfected MES13 cells. The p3xFLAG-FOXD1 expression construct was generated by subcloning mouse *Foxd1* cDNA into a mammalian expression vector along with an N-terminal triple FLAG epitope (3xFLAG). The Imprint Ultra Chromatin Immunoprecipitation Kit (Sigma-Aldrich) was used with a rabbit anti-FLAG monoclonal antibody (Sigma-Aldrich, M8823) according to the manufacturer's instructions.

Acknowledgements

We thank Professor Liliana Schaefer for help in importing the decorin null mouse strain.

Competing interests

The authors declare no competing financial interests.

Author contributions

J.L.F. and L.O. designed research; J.L.F., J.A.G., M.J.K., D.C.A. and D.E.M. performed research; R.V.I. and A.C.B. contributed reagents/analytic tools; J.L.F. and L.O. analyzed data; and J.L.F. and L.O. wrote the paper.

Funding

This work was supported by the National Institutes of Diabetes and Digestive and Kidney Disease (NIDDK) [R01DK078161 to L.O. and an American Recovery and Reinvestment Act (ARRA)-supported supplement to R01DK078161]. Additional support was provided by an NIDDK F32 fellowship [F32DK093196 to J.L.F.]; a predoctoral fellowship from the American Heart Association (J.A.G.) and a postdoctoral fellowship from the American Heart Association (A.C.B.). Core facilities support was provided by Maine Medical Center Research Institute core facilities for Molecular Phenotyping [supported by National Institutes of General Medicine (NIGM) 8P30 GM106391], Histopathology [NIGM 8P30 GM106391 and 8P30 GM103392], the Mouse Transgenic and *In Vivo* Core [NIGM 8P30 GM103392], the Cell Imaging Core [NIGM 8P30 GM103392] and by the Microarray Facility of the Vermont Genetics Network [NIGM 8P20GM103449]. Deposited in PMC for release after 12 months.

Supplementary material

Supplementary material available online at
http://dev.biologists.org/lookup/suppl/doi:10.1242/dev.089078/-/DC1

References

Alexi, X., Berditchevski, F. and Odintsova , E. (2011). The effect of cell-ECM adhesion on signalling via the ErbB family of growth factor receptors. *Biochem. Soc. Trans.* **39**, 568-573.

Ang, S. L. and Rossant, J. (1994). HNF-3 beta is essential for node and notochord formation in mouse development. *Cell* **78**, 561-574.

Barak, H. and Boyle, S. C. (2011). Organ culture and immunostaining of mouse embryonic kidneys. *Cold Spring Harb. Protoc.* **2011**, pdb prot5558.

Behr, R., Sackett, S. D., Bochkis, I. M., Le, P. P. and Kaestner, K. H. (2007). Impaired male fertility and atrophy of seminiferous tubules caused by haploinsufficiency for Foxa3. *Dev. Biol.* **306**, 636-645.

Blank, U., Brown, A., Adams, D. C., Karolak, M. J. and Oxburgh, L. (2009). BMP7 promotes proliferation of nephron progenitor cells via a JNK-dependent mechanism. *Development* **136**, 3557-3566.

Brown, A. C., Adams, D., de Caestecker, M., Yang, X., Friesel, R. and Oxburgh, L. (2011). FGF/EGF signaling regulates the renewal of early nephron progenitors during embryonic development. *Development* **138**, 5099-5112.

Brown, A. C., Muthukrishnan, S. D., Guay, J. A., Adams, D. C., Schafer, D. A., Fetting, J. L. and Oxburgh, L. (2013). Role for compartmentalization in nephron progenitor differentiation. *Proc. Natl. Acad. Sci. USA* **110**, 4640-4645.

Chi, X., Michos, O., Shakya, R., Riccio, P., Enomoto, H., Licht, J. D., Asai, N., Takahashi, M., Ohgami, N., Kato, M. et al. (2009). Ret-dependent cell rearrangements in the Wolffian duct epithelium initiate ureteric bud morphogenesis. *Dev Cell* **17**, 199-209.

Danielson, K. G., Baribault, H., Holmes, D. F., Graham, H., Kadler, K. E. and Iozzo, R. V. (1997). Targeted disruption of decorin leads to abnormal collagen fibril morphology and skin fragility. *J. Cell Biol.* **136**, 729-743.

Das, A., Tanigawa, S., Karner, C. M., Xin, M., Lum, L., Chen, C., Olson, E. N., Perantoni, A. O. and Carroll, T. J. (2013). Stromal-epithelial crosstalk regulates kidney progenitor cell differentiation. *Nat. Cell Biol.* **15**, 1035-1044.

Edgar, R., Domrachev, M. and Lash, A. E. (2002). Gene Expression Omnibus: NCBI gene expression and hybridization array data repository. *Nucleic Acids Res.* **30**, 207-210.

Fleischmajer, R., Fisher, L. W., MacDonald, E. D., Jacobs, L., Jr, Perlish, J. S. and Termine, J. D. (1991). Decorin interacts with fibrillar collagen of embryonic and adult human skin. *J. Struct. Biol.* **106**, 82-90.

Fontenot, J. D., Gavin, M. A. and Rudensky, A. Y. (2003). Foxp3 programs the development and function of CD4+CD25+ regulatory T cells. *Nat. Immunol.* **4**, 330-336.

Gajiwala, K. S. and Burley, S. K. (2000). Winged helix proteins. *Curr. Opin. Struct. Biol.* **10**, 110-116.

Guzman, A., Zelman-Femiak, M., Boergermann, J. H., Paschkowsky, S., Kreuzaler, P. A., Fratzl, P., Harms, G. S. and Knaus, P. (2012). SMAD versus non-SMAD signaling is determined by lateral mobility of bone morphogenetic protein (BMP) receptors. *J. Biol. Chem.* **287**, 39492-39504.

Hannenhalli, S. and Kaestner, K. H. (2009). The evolution of Fox genes and their role in development and disease. *Nat. Rev. Genet.* **10**, 233-240.

Harding, S. D., Armit, C., Armstrong, J., Brennan, J., Cheng, Y., Haggarty, B., Houghton, D., Lloyd-MacGilp, S., Pi, X., Roochun, Y. et al. (2011). The GUDMAP database – an online resource for genitourinary research. *Development* **138**, 2845-2853.

Hartwig, S., Bridgewater, D., Di Giovanni, V., Cain, J., Mishina, Y. and Rosenblum, N. D. (2008). BMP receptor ALK3 controls collecting system development. *J. Am. Soc. Nephrol.* **19**, 117-124.

Hatini, V., Huh, S. O., Herzlinger, D., Soares, V. C. and Lai, E. (1996). Essential role of stromal mesenchyme in kidney morphogenesis revealed by targeted disruption of Winged Helix transcription factor BF-2. *Genes Dev.* **10**, 1467-1478.

Huang, W., Sherman, B. T. and Lempicki, R. A. (2009a). Bioinformatics enrichment tools: paths toward the comprehensive functional analysis of large gene lists. *Nucleic Acids Res.* **37**, 1-13.

Huang, W., Sherman, B. T. and Lempicki, R. A. (2009b). Systematic and integrative analysis of large gene lists using DAVID bioinformatics resources. *Nat. Protoc.* **4**, 44-57.

Humphreys, B. D., Lin, S. L., Kobayashi, A., Hudson, T. E., Nowlin, B. T., Bonventre, J. V., Valerius, M. T., McMahon, A. P. and Duffield, J. S. (2010). Fate tracing reveals the pericyte and not epithelial origin of myofibroblasts in kidney fibrosis. *Am. J. Pathol.* **176**, 85-97.

Ichii, M., Frank, M. B., Iozzo, R. V. and Kincade, P. W. (2012). The canonical Wnt pathway shapes niches supportive of hematopoietic stem/progenitor cells. *Blood* **119**, 1683-1692.

Iozzo, R. V. and Schaefer, L. (2010). Proteoglycans in health and disease: novel regulatory signaling mechanisms evoked by the small leucine-rich proteoglycans. *FEBS J.* **277**, 3864-3875.

Karner, C. M., Das, A., Ma, Z., Self, M., Chen, C., Lum, L., Oliver, G. and Carroll, T. J. (2011). Canonical Wnt9b signaling balances progenitor cell expansion and differentiation during kidney development. *Development* **138**, 1247-1257.

Korchynskyi, O. and ten Dijke, P. (2002). Identification and functional characterization of distinct critically important bone morphogenetic protein-specific response elements in the Id1 promoter. *J. Biol. Chem.* **277**, 4883-4891.

Lai, C. S., Fisher, S. E., Hurst, J. A., Vargha-Khadem, F. and Monaco, A. P. (2001). A forkhead-domain gene is mutated in a severe speech and language disorder. *Nature* **413**, 519-523.

Lee, C. S., Friedman, J. R., Fulmer, J. T. and Kaestner, K. H. (2005). The initiation of liver development is dependent on Foxa transcription factors. *Nature* **435**, 944-947.

Levinson, R. S., Batourina, E., Choi, C., Vorontchikhina, M., Kitajewski, J. and Mendelsohn, C. L. (2005). Foxd1-dependent signals control cellularity in the renal capsule, a structure required for normal renal development. *Development* **132**, 529-539.

Lindahl, P., Hellström, M., Kalén, M., Karlsson, L., Pekny, M., Pekna, M., Soriano, P. and Betsholtz, C. (1998). Paracrine PDGF-B/PDGF-Rbeta signaling controls mesangial cell development in kidney glomeruli. *Development* **125**, 3313-3322.

Mathews, S., Bhonde, R., Gupta, P. K. and Totey, S. (2012a). Extracellular matrix protein mediated regulation of the osteoblast differentiation of bone marrow derived human mesenchymal stem cells. *Differentiation* **84**, 185-192.

Mathews, S., Mathew, S. A., Gupta, P. K., Bhonde, R. and Totey, S. (2012b). Glycosaminoglycans enhance osteoblast differentiation of bone marrow derived human mesenchymal stem cells. *J. Tissue Eng. Regen. Med.* [Epub ahead of print] doi: 10.1002/term.1507.

McMahon, A. P., Aronow, B. J., Davidson, D. R., Davies, J. A., Gaido, K. W., Grimmond, S., Lessard, J. L., Little, M. H., Potter, S. S., Wilder, E. L. et al.; GUDMAP project (2008). GUDMAP: the genitourinary developmental molecular anatomy project. *J. Am. Soc. Nephrol.* **19**, 667-671.

Mugford, J. W., Yu, J., Kobayashi, A. and McMahon, A. P. (2009). High-resolution gene expression analysis of the developing mouse kidney defines novel cellular compartments within the nephron progenitor population. *Dev. Biol.* **333**, 312-323.

Nakae, J., Biggs, W. H., III, Kitamura, T., Cavenee, W. K., Wright, C. V., Arden, K. C. and Accili, D. (2002). Regulation of insulin action and pancreatic beta-cell function by mutated alleles of the gene encoding forkhead transcription factor Foxo1. *Nat. Genet.* **32**, 245-253.

Neill, T., Schaefer, L. and Iozzo, R. V. (2012). Decorin: a guardian from the matrix. *Am. J. Pathol.* **181**, 380-387.

Overdier, D. G., Porcella, A. and Costa, R. H. (1994). The DNA-binding specificity of the hepatocyte nuclear factor 3/forkhead domain is influenced by amino-acid residues adjacent to the recognition helix. *Mol. Cell. Biol.* **14**, 2755-2766.

Oxburgh, L., Chu, G. C., Michael, S. K. and Robertson, E. J. (2004). TGFbeta superfamily signals are required for morphogenesis of the kidney mesenchyme progenitor population. *Development* **131**, 4593-4605.

Park, J. S., Ma, W., O'Brien, L. L., Chung, E., Guo, J. J., Cheng, J. G., Valerius, M. T., McMahon, J. A., Wong, W. H. and McMahon, A. P. (2012). Six2 and Wnt regulate self-renewal and commitment of nephron progenitors through shared gene regulatory networks. *Dev. Cell* **23**, 637-651.

Parkin, J. D., San Antonio, J. D., Pedchenko, V., Hudson, B., Jensen, S. T. and Savige, J. (2011). Mapping structural landmarks, ligand binding sites, and missense mutations to the collagen IV heterotrimers predicts major functional domains, novel interactions, and variation in phenotypes in inherited diseases affecting basement membranes. *Hum. Mutat.* **32**, 127-143.

Pierrou, S., Hellqvist, M., Samuelsson, L., Enerbäck, S. and Carlsson, P. (1994). Cloning and characterization of seven human forkhead proteins: binding site specificity and DNA bending. *EMBO J.* **13**, 5002-5012.

Schaefer, L. and Iozzo, R. V. (2008). Biological functions of the small leucine-rich proteoglycans: from genetics to signal transduction. *J. Biol. Chem.* **283**, 21305-21309.

Schönherr, E., Hausser, H., Beavan, L. and Kresse, H. (1995). Decorin-type I collagen interaction. Presence of separate core protein-binding domains. *J. Biol. Chem.* **270**, 8877-8883.

Sebinger, D. D., Ofenbauer, A., Gruber, P., Malik, S. and Werner, C. (2013). ECM modulated early kidney development in embryonic organ culture. *Biomaterials* **34**, 6670-6682.

Shih, D. Q., Navas, M. A., Kuwajima, S., Duncan, S. A. and Stoffel, M. (1999). Impaired glucose homeostasis and neonatal mortality in hepatocyte nuclear factor 3alpha-deficient mice. *Proc. Natl. Acad. Sci. USA* **96**, 10152-10157.

Shu, W., Cho, J. Y., Jiang, Y., Zhang, M., Weisz, D., Elder, G. A., Schmeidler, J., De Gasperi, R., Sosa, M. A., Rabidou, D. et al. (2005). Altered ultrasonic vocalization in mice with a disruption in the Foxp2 gene. *Proc. Natl. Acad. Sci. USA* **102**, 9643-9648.

Wan, H., Dingle, S., Xu, Y., Besnard, V., Kaestner, K. H., Ang, S. L., Wert, S., Stahlman, M. T. and Whitsett, J. A. (2005). Compensatory roles of Foxa1 and Foxa2 during lung morphogenesis. *J. Biol. Chem.* **280**, 13809-13816.

Wang, X., Harimoto, K., Xie, S., Cheng, H., Liu, J. and Wang, Z. (2010). Matrix protein biglycan induces osteoblast differentiation through extracellular signal-regulated kinase and Smad pathways. *Biol. Pharm. Bull.* **33**, 1891-1897.

Yaklichkin, S., Steiner, A. B., Lu, Q. and Kessler, D. S. (2007a). FoxD3 and Grg4 physically interact to repress transcription and induce mesoderm in Xenopus. *J. Biol. Chem.* **282**, 2548-2557.

Yaklichkin, S., Vekker, A., Stayrook, S., Lewis, M. and Kessler, D. S. (2007b). Prevalence of the EH1 Groucho interaction motif in the metazoan Fox family of transcriptional regulators. *BMC Genomics* **8**, 201.

Yamaguchi, Y., Mann, D. M. and Ruoslahti, E. (1990). Negative regulation of transforming growth factor-beta by the proteoglycan decorin. *Nature* **346**, 281-284.

Yu, J., Carroll, T. J., Rajagopal, J., Kobayashi, A., Ren, Q. and McMahon, A. P. (2009). A Wnt7b-dependent pathway regulates the orientation of epithelial cell division and establishes the cortico-medullary axis of the mammalian kidney. *Development* **136**, 161-171.

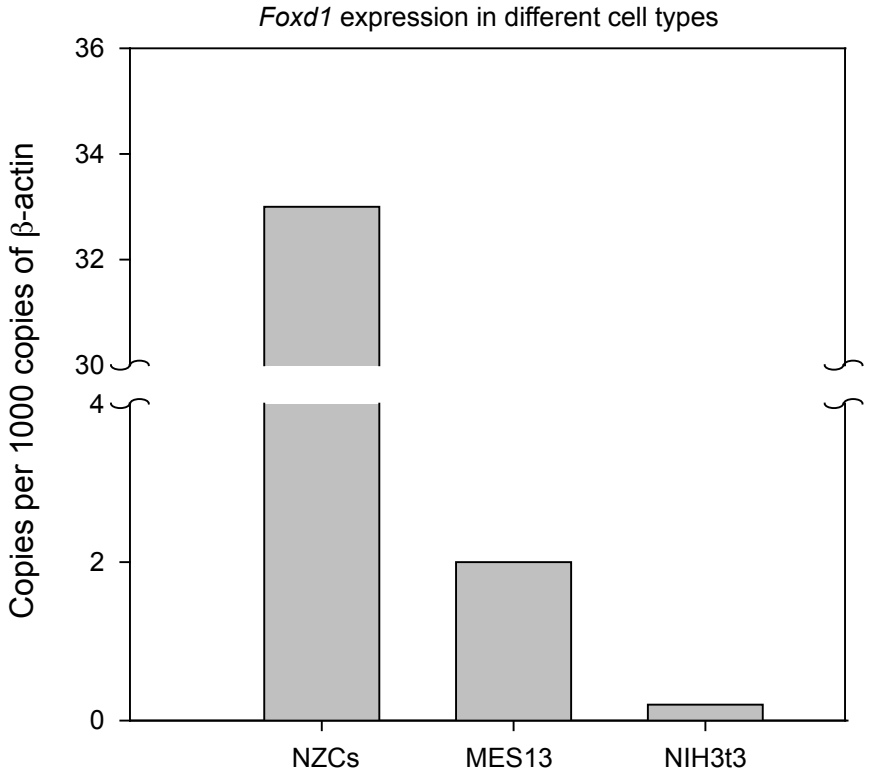

Figure S1. Bar graph depicting number of copies of *Foxd1* per 1000 copies of β-actin in nephrogenic zone cells (NZCs), MES13 cells, and NIH3T3 cells.

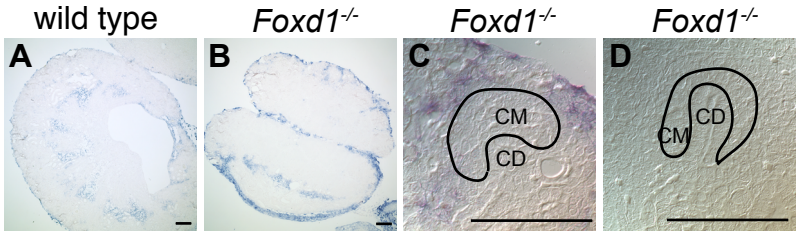

Figure S2. *Dcn* overexpression in *Foxd1*$^{-/-}$ kidneys decreases by E17.5. (A) In situ hybridization with a probe against *Dcn* reveals *Dcn* is expressed in the capsule and medullary interstitium in E17.5 wild type kidneys. (B) *Dcn* overexpression is reduced in interstitium in *Foxd1*$^{-/-}$ kidneys compared to E14.5 (Fig. 3C,D). (C,D) 100x image *Foxd1*$^{-/-}$ kidney. Large cap mesenchyme (CM) complexes are adjacent to aberrant *Dcn* expression, while other smaller clusters (D) are not surrounded by Dcn expressing cells. CD = collecting duct .Scale bar = 100μm.

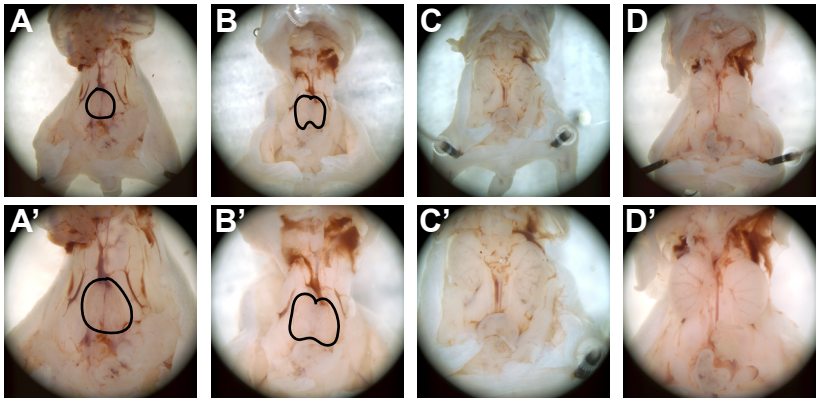

Figure S3. Ablation of *Dcn* does not rescue the *Foxd1*$^{-/-}$ horseshoe kidney phenotype. (A, A') *Foxd1*$^{-/-}$;*Dcn*$^{-/-}$ kidneys are fused into a horseshoe shape along the dorsal midline (outlined in black). (B, B') *Foxd1-/-* kidneys have the same characteristic horseshoe shape. (C, C') *Dcn*$^{-/-}$ kidneys separate normally. (D, D') Wild-type kidneys separate normally.

Dcn-luc1 F	ATCGATCTCGAGTGGACATAATTCTGGTGCCATCT
Dcn-luc1 R	ATCGATAGATCTTGCTTTATCAAGAGGCTTGCTTT
Dcn-luc2 F	ATCGATCTCGAGGGGATCAAAATTGCATCTCACA
Dcn-luc2 R	ATCGATAGATCTTGTAGAGAAATGAGCCTATGTGT
Dcn-luc3 F	ATCGATAGATCTTGTAGAGAAATGAGCCTATGTGT
Dcn-luc3 R	ATCGATAGATCTATGCTTGCCTCACTACTGCC
Dcn-luc2-mut F	GCGCGCTGCAGACATGACCTGCATCTGAATGCTCCAAAGCCGGTAGGATGTTAGCTT
Dcn-luc2-mut R	TGCAGGTCATGTCTGCAGTGTGTGTTGAATTCAGGG
Dcn F primer (T3)	CCAAGCCTTCATTAACCCTCACTAAAGGGAGACCTCCTTCTTTCCACACCTG
Dcn R primer (T7)	CAGAGATGCATAATACGACTCACTATAGGGAGACCATAACGGTGATGCTGTTG
5’ binding site primer (F)	TTTCATACCCTCCCCTGAAA
5’ binding site primer (R)	CAGGGCATTTGCTTTTCCTA
3’ binding site primer (F)	CCGTACACTTTCGCAGAACA
3’ binding site primer (R)	GAGAGCAAAGGCATCCA

Fetting_TableS1

Table S2. Microarray Analysis of E14.5 wild type and *Foxd1*$^{-/-}$ kidneys			
Gene	NCBI #	FC	P-value
Sulf1	NM_172294	3.88E+00	8.01E-04
Mgp	NM_008597	3.87E+00	8.81E-04
Actg2	NM_009610	2.95E+00	7.28E-03
Acta2	NM_007392	2.78E+00	1.70E-03
Prrx1	NM_175686	2.72E+00	7.14E-03
Epha3	NM_010140	2.63E+00	3.65E-04
Slc26a7	NM_145947	2.58E+00	9.58E-04
Sqrdl	NM_021507	2.54E+00	7.83E-03
Dcn	NM_007833	2.49E+00	2.00E-04
Fbln5	NM_011812	2.46E+00	5.54E-03
Pi15	NM_053191	2.40E+00	8.95E-03
Lox	NM_010728	2.39E+00	1.12E-03
Grin3a	NM_001033351	2.32E+00	2.46E-03
Col12a1	NM_007730	2.32E+00	8.28E-04
Enpp1	NM_008813	2.31E+00	1.88E-03
Col14a1	NM_181277	2.13E+00	2.84E-03
Olfr78	NM_130866	2.04E+00	2.72E-03
Thbs2	NM_011581	2.04E+00	4.99E-04
Prdm6	NM_001033281	1.98E+00	9.02E-03
Plcxd3	NM_177355	1.98E+00	8.11E-03
Dclk1	NM_019978	1.96E+00	2.32E-03
Pcdh7	NM_018764	1.95E+00	8.67E-03
Angpt2	NM_007426	1.92E+00	1.04E-03
Col1a2	NM_007743	1.91E+00	5.18E-03
Maob	NM_172778	1.90E+00	9.31E-03
Ccl11	NM_011330	1.83E+00	5.88E-03
Fbn1	NM_007993	1.83E+00	5.05E-03
Rgs5	NM_009063	1.75E+00	8.21E-03
Col1a1	NM_007742	1.72E+00	2.14E-03
Gria3	NM_016886	1.72E+00	7.69E-03
Gas2	NM_008087	1.68E+00	8.66E-03
9130213b05rik	BC006604	1.65E+00	8.07E-03
Pde1a	NM_016744	1.65E+00	2.28E-03
Ednra	NM_010332	1.65E+00	5.74E-03
Ltbp1	NM_019919	1.63E+00	1.05E-03
Svep1	NM_022814	1.62E+00	3.15E-03
Fkbp9	NM_012056	1.62E+00	2.08E-03
Ednrb	NM_007904	1.60E+00	5.49E-03
Abca1	NM_013454	1.59E+00	5.94E-03
Col6a1	NM_009933	1.58E+00	7.72E-03
Sparcl1	NM_010097	1.57E+00	5.10E-03
e330026b02rik	NM_172927	1.56E+00	3.90E-03
Mfap5	NM_015776	1.53E+00	9.90E-03
Bmper	NM_028472	1.53E+00	7.65E-03
Upk1b	NM_178924	1.51E+00	2.63E-03

Fbln2	NM_007992	1.50E+00	5.63E-03
Crispld1	NM_031402	1.50E+00	8.76E-03
Zeb2	NM_015753	1.49E+00	1.17E-03
Ssbp2	NM_024272	1.49E+00	8.17E-03
Itgb6	NM_021359	-1.45E+00	9.60E-03
Plch1	NM_183191	-1.50E+00	1.69E-03
Mme	NM_008604	-1.52E+00	5.04E-04
Grb7	NM_010346	-1.56E+00	6.20E-03
Mal	NM_010762	-1.57E+00	4.25E-04
Hnf4a	NM_008261	-1.60E+00	6.91E-03
Svopl	NM_177200	-1.60E+00	3.48E-03
Lama1	NM_008480	-1.61E+00	2.72E-03
Tpmt	NM_016785	-1.62E+00	7.92E-03
Hrsp12	NM_008287	-1.65E+00	5.34E-03
Slc7a9	NM_021291	-1.66E+00	7.45E-03
Ppargc1a	NM_008904	-1.66E+00	9.56E-03
Cryz	NM_009968	-1.69E+00	5.59E-03
Emx2	NM_010132	-1.69E+00	6.42E-03
Myb	NM_010848	-1.70E+00	5.43E-03
Gipc2	NM_016867	-1.70E+00	3.44E-03
Dsp	NM_023842	-1.71E+00	7.09E-03
Cys1	NM_138686	-1.72E+00	3.65E-03
Esrrg	NM_011935	-1.73E+00	5.02E-03
Sim1	NM_011376	-1.77E+00	2.76E-04
Ntm	NM_172290	-1.78E+00	1.48E-03
Cyp4a10	NM_010011	-1.81E+00	1.58E-03
Tinag	NM_012033	-1.82E+00	3.70E-03
Vil1	NM_009509	-1.83E+00	6.80E-03
Sostdc1	NM_025312	-1.84E+00	2.30E-03
Ggt1	NM_008116	-1.85E+00	2.62E-03
Aldh1a2	NM_009022	-1.85E+00	5.08E-04
Cpa2	NM_001024698	-1.88E+00	2.57E-03
Fut9	NM_010243	-1.88E+00	6.79E-04
Eg381483	ENSMUST00000092878	-1.89E+00	2.40E-03
Rbm47	NM_178446	-1.90E+00	9.97E-03
Erbb4	NM_010154	-1.94E+00	4.30E-03
Tmem27	NM_020626	-1.97E+00	4.23E-03
Fggy	NM_001113412	-2.06E+00	4.11E-03
Cdh6	NM_007666	-2.08E+00	1.21E-03
Myo5b	NM_201600	-2.08E+00	6.67E-04
Dcdc2a	NM_177577	-2.11E+00	2.02E-03
Dkk1	NM_010051	-2.13E+00	2.99E-03
Cyp4a32	ENSMUST00000084342	-2.14E+00	8.08E-03
Aldob	NM_144903	-2.18E+00	1.77E-03
1700011h14rik	BC026534	-2.21E+00	3.29E-03
Lhx1	NM_008498	-2.21E+00	2.16E-03
Fxyd2	NM_007503	-2.36E+00	7.47E-03

pdzk1	NM_021517	-2.38E+00	1.83E-03
cpb2	NM_019775	-2.47E+00	3.59E-03
atp1b1	NM_009721	-2.56E+00	5.48E-03
hnf1b	NM_009330	-2.56E+00	2.32E-03
osr2	NM_054049	-2.57E+00	8.20E-03
anxa13	NM_027211	-2.58E+00	1.30E-03
anks4b	NM_028085	-2.72E+00	4.88E-03
lrp2	NM_001081088	-2.82E+00	4.85E-03
mep1a	NM_008585	-3.02E+00	2.66E-03
cyp4a31	ENSMUST00000030480	-3.02E+00	1.59E-03
keg1	BC010803	-3.17E+00	2.95E-03
d630042f21rik	BC120661	-3.22E+00	2.27E-03
cldn1	NM_016674	-3.27E+00	2.68E-03
car4	NM_007607	-3.29E+00	1.33E-04
slc12a1	NM_183354	-3.45E+00	4.50E-03
dpp4	NM_010074	-3.49E+00	2.46E-03
sult1d1	NM_016771	-3.72E+00	9.40E-03

Gene name	Binding site
pDcn-luc1 transcription factors binding sites	
V$GATA_C	cgttcTTATCt
V$GATA1_04	gttcTTATCttcc
V$GATA1_05	tcTTATCttc
V$GATA1_06	tcTTATCTtc
V$GATA2_02	tcTTATCttc
V$GATA2_03	TCTTATCttc
V$GATA3_02	tcTTATCttc
V$GATA6_01	tcttATCttc
V$GATA_Q6	ctTATCt
V$HNF1_C	aGTTAACAAGTCAccta
V$BACH1_01	accATTAGTAATgct
V$NFY_Q6	gagCCAATctt
V$HOXA7_01	cCAATCT
V$E2F1_Q4_01	agCACCAAA
V$E2F_Q3_01	agCACCAAA
V$E2F1DP1RB_01	GCACCAAA
V$E2F4DP1_01	GCACCAAA
V$E2F_02	GCACCAAA
V$E2F_Q3	GCACCAAA
V$E2F_Q4	gCACCAAA
V$PAX5_02	aatgtgATCGTGCTCCAAGTTTCttttg
V$EGR_Q6	gttgTCCCCAC
V$OCT1_03	tccTAATTAtaag
V$CDXA_02	tataAat
V$GATA6_01	aatGATaagt
V$GATA_Q6	tGATAag
V$XVENT1_01	gtaatATTTGctc
pDcn-luc2 transcription factor binding sites	
V$OCT_C	tTCATTTGCCTtt
V$IRF1_01	gcATTTGCTTTtc
V$XFD3_01	agaaTATTTACaga
V$SRF_Q6	gaCCAAATAGGTgc
V$HOXA3_01	ccaaatAgg
V$P53_DECAMER_Q2	agaCATGacc
V$ER_Q6_02	gacaTGACCTg
V$ERR1_Q2	caTGACCTgcatct
V$RORA1_01	aTGACCTgcatct
V$RORA2_01	aTGACCTGCATct
V$E2F1DP1RB_01	GCTCCAAA
V$E2F4DP1_01	GCTCCAAA
V$E2F_02	GCTCCAAA
V$E2F_Q3	GCTCCAAA
V$E2F_Q4	gCTCCAAA
V$FREAC4_01	CCAAAGTCAACAggat
V$CETS1P54_01	aCAGGAtgtt